IOP Conf. Series: Materials Science and Engineering **181** (2017) 012027 doi:10.1088/1757-899X/181/1/012027

Investigation of the effect of contaminations and cleaning processes on the surface properties of brazing surfaces

K Bobzin[1], M Öte[1] and S Wiesner[1,2]

[1]Surface Engineering Institute, RWTH Aachen University, Aachen, Germany
[2]wiesner@iot.rwth-aachen.de

Abstract. The quality of brazed joints is determined by different factors such as the atmosphere and the parameters during brazing as well as the condition of the brazing surfaces. Residues of lubricants used during machining of the components and the subsequent cleaning processes can contaminate the faying surfaces and can hence influence the flow ability of the molten filler metals. Besides their influence on the filler metal flow, the residues can result in the formation of carbonic phases in the joint leading to a possible reduction of the corrosion resistance and the mechanical properties. The first step of the current study with the aim of avoiding these defects is to identify the influence of critical contaminations and cleaning methods on the quality of the brazed joints. In a first step, contaminations on AISI304 and Inconel alloy 625 due to different cooling lubricants and the effect of several cleaning methods, in particular plasma cleaning, have been investigated. Information about the surface energy of contaminated and cleaned surfaces was gained by measuring contact angle of testing fluids. Additionally, the lubricants and the resulting contamination products have been analyzed considering the influence of a heat treatment.

1. Introduction

Technical components processed by brazing are usually subjected to different machining processes prior to brazing. On the faying surfaces contaminations from the machining process such as machining oils and emulsions, swarfs, drawing greases, polishes and degradation products can be found [1, 2]. These contaminations are critical for the wetting behavior of the filler metal during the brazing process. If the surface is not sufficiently free from oxides and contaminations, the molten filler metal cannot wet the complete brazing surface. The result of the insufficient wetting is the formation of voids and porosity in the brazed joint, reducing its mechanical properties and also the corrosion resistant of the whole compound.

Therefore, the components to be brazed pass through a cleaning process consisting of different steps and different mechanical, thermal and chemical cleaning processes depending on the type of contamination. Basic information about possible cleaning processes can be found in DIN 8592 [3]. Often, chemical cleaning agents based on organic solvents or water-based cleaning agents are used in ultrasonic baths to dissociate the contamination particles from the surfaces and to transfer the energy from the cleaning bath in terms of heat or ultrasonic waves to the components. Additionally, treatments with cold atmospheric plasmas recently gain more significance for cleaning processes as this method can be applied for nearly all types of materials. As only small amounts of organic contaminations $m < 0{,}5\ g/m^2$ [4] can be efficiently removed from the surfaces by means of cold atmospheric plasmas, the plasma treatment is conducted usually as the last step in the cleaning process

resulting in very clean surfaces [5]. The carbonic contaminations on the surface are converted by means of the plasma into CO_2 and thus removed from the surface.

While the importance of the pre-cleaning of the components for the quality of the brazed joint is known, there is neither systematic information about the efficiency of the cleaning processes nor a recommended practice for an acceptable type and degree of contamination. Additionally, the behavior of the contaminations during the brazing process is unknown. Therefore, this study focuses on the investigation of the change of surface energy of the common base materials for brazing, X15CrNi18-10 and IN 625, with respect to the surface roughness and the cleaning process. The cleaning process includes pre-cleaning with chemical agents and a subsequent plasma treatment. Additionally, the behavior of contaminations from mineral oil-containing and synthetic lubricants is analyzed, considering the heat treatment conditions, which are comparable with those occurring during a brazing process.

2. Materials and Experimental Procedure

Two base materials, the stainless steel X5CrNi18-10 (1.4301, AISI 304) and the nickel-based super alloy INCONEL® 625 (IN 625) were used in this study. X5CrNi18-10 is an austenitic corrosion-resistant steel that has a wide application range for example in automotive industry and mechanical engineering. IN 625 is a corrosion-resistant nickel-based alloy that is used for components operating at elevated temperatures such as turbine blades due to its high oxidation resistance and good mechanical properties. Both materials are often brazed in industrial practice. The composition of the base materials is listed in table 1.

Table 1. Composition of the base materials X5CrNi18-10 and IN 625 in wt.-%.

	Fe	Ni	Cr	Mo	Mn	Si	C	P	S	N	Al
X5CrNi18-10	≥ 66,8	8-10,5	17-19,5	-	≤ 2	≤ 1	≤ 0,07	≤ 0,045	≤ 0,015	≤ 0,11	-
IN 625	≤ 5	≥ 58	20-23	8-10	≤ 0,5	≤ 0,5	≤ 0,1	≤ 0,015	≤ 0,015	≤ 0,4	≤ 0,4

For this study, substrates were cut from metal sheets made of X15CrNi18-10 and IN 625 in the dimensions of V = 20 mm x 25 mm x 5 mm. After cutting, the samples were milled or manually ground with SiC papers with grit sizes between 180 and 1,200 to generate a variety of the substrate roughnesses. The roughness of the sample surfaces was measured by a confocal laser scanning microscope of the type VKX 210, Keyence (Osaka, Japan) according to DIN EN ISO 25178 [6]. The area-related roughness values Sz and Sa were measured, corresponding with Rz and Ra from profile measurements. For each sample type, at least five measurements were used to calculate average roughness values.

In order to achieve samples with a surface contamination comparable to industrial practice, the cooling lubricants Avialub V3352 and Avia Metacool Syntogrind were used for milling the samples. The content of mineral oil in Avialub, which is a common lubricant for various machining operations, amounts to around 17 %. Avia Metacool, which is a synthetic, mineral oil-free lubricant, is mostly used for grinding and machining steel components. A mixture of 10 vol.-% lubricant and 90 vol.-% demineralized water was applied on the samples to create contaminated surfaces. As a more complex reference contamination, a variation of the Shell standard contamination [1] was used with the following composition:

- 35 wt.-% lanoline
- 25 wt.-% lithium stearate ($C_{18}H_{35}LiO_2$) as a typical compound of lithium soap used as lubricant grease
- 20 % corrosion protection liquid BRANOtect Export
- 10 % polydimethylsiloxane, a member of silicon oils used as lubricants
- 10 % Fe(III) oxide representing chips or shaving from the machining process.

The lubricants and the reference were applied on the milled and ground samples until a homogeneous layer of contamination forms on the surface. Subsequently, the samples were dried for t_{drying} = 30 min in ambient atmosphere. Some samples were analyzed in contaminated state and the rest subsequent to the respective cleaning operation.

As chemical cleaning agents Aceton and IBS-Spezialreiniger EL/Extra, referred to as "IBS" henceforth, were used in this study. IBS is a cleaning agent based on non-halogenated, isoparaffinic, aliphatic hydrocarbons. The cleaning process for the contaminated samples includes a cleaning step in an ultrasonic bath with the respective cleaning agent for $t_{cleaning}$ = 15 min at $T_{cleaning}$ = 30 °C, followed by a rinse cycle in demineralized water resulting in a homogeneous clean surface.

For plasma cleaning, CAT Compact device of Tigres GmbH (Marschacht, Germany) was used. This device generates an almost potential-free atmospheric plasma that can degrease, clean and activated metallic surfaces. The plasma is operated using compressed air as process gas at a net power of P = 600 W. The cleaning device was installed on an industrial robot head moving according to a programmed meandering profile with a velocity of v = 5 mm/s. Based on the plasma nozzle diameter of $\square_{nozzle}$ = 4 mm, the distance between the meanders was chosen to be s = 4 mm. Thus, a homogenous treatment of the substrate surface could be ensured. The gap between the nozzle and the sample surface was about d = 5 mm. In order to achieve a stronger cleaning effect, the plasma treatment was conducted twice on the same surface.

The heat treatment of the samples was performed with a temperature-time profile comparable to the brazing process. It was realized in high vacuum with a pressure of $p < 5 \cdot 10^{-5}$ mbar in a PVA MOV 553 T furnace of PVA TePla AG (Wettenberg, Germany). The heating rate was $\dot{T}$ = 10 K/min up to T = 1.100 °C for t = 10 min.

The cleanliness of the sample surfaces was at first roughly analyzed by the CleanoSpector from SITA Messtechnik GmbH (Dresden, Germany), a device measuring the fluorescence of surface contaminations. The substances on the surface are activated by ultraviolet light in order to bring these to exhibit fluorescence, which in turn is detected by the device and compared with the intensity of emissions of a standard clean surface. The result is given in percentage cleanliness compared to the cleanliness of the standard surface. A lower intensity of fluorescence compared to the clean surface results in a cleanliness value above 100 %. This measurement method is generally suitable for detecting organic and carbon-based substances, but has also proven to be efficient for perceiving mineral oil based contaminations [7, 8]. Due to the rapidity and facility of the measurement, it is used in industrial practice to evaluate roughly, if the cleanliness of the components delivered by the supplier is suitable for the following brazing process.

In order to determine the surface energy of the cooling lubricants and the sample surfaces, contact angle measurements were performed by means of a DSA 10 video device of KRÜSS GmbH (Hamburg, Germany). The surface energy was calculated using the translational angle of several test liquids that were dynamically measured. As test liquids, demineralized water, diiodomethane, ethylene glycol and glycerin were chosen due to their differing polar and disperse components of the surface energy [9, 10]. For every surface condition and every test liquid, at least five measurements were conducted.

The samples with fresh and heat-treated lubricants were analyzed by means of Micro-Raman spectroscopy. For this analysis, an inVia Reflex spectroscope by Renishaw GmbH (Pliezhausen, Germany) was used. The employed YAG laser had a wavelength of λ = 532 nm and the Raman shift in the range of $500\ cm^{-1} \leq \tilde{\upsilon} \leq 3{,}200\ cm^{-1}$ was determined. The scans were performed five times to achieve statistically reliable results.

Additionally, combined differential scanning calorimetric (DSC) and thermogravimetric (TG) measurements were conducted to analyze the behaviour of the lubricants during the heat treatment process. The focus of this analysis was mainly the investigation of the weight loss by evaporation or decomposition of compounds in the lubricants. For the DSC/TG measurements, the thermoanalytic system Setaram SetSys Evolution 16/18 of Setaram Instrumentation (Caluire, Frankreich) was used. Around m = 20 mg of the lubricants was placed in Al_2O_3 crucibles and heated up in an argon

atmosphere with a heating rate of $\dot{T}$ = 10 K/min up to temperature of T = 800 °C. The heat flow as a result of the DSC analysis is recorded and the weight change in % is calculated from a tared weight signal.

3. Results and Discussion

First, the influence of the roughness on the surface energy of the substrate materials was determined by contact angle measurements. Additionally, the effect of plasma treatment of contaminated and pre-cleaned surfaces on the cleanliness was determined. It can be expected that the heat treatment, for example during brazing process, significantly influences the chemical composition of the lubricants and the formation of residues on the sample surfaces. Hence, contaminated samples were heat treated and analyzed by combined DSC/TG measurements and Micro-Raman spectroscopy.

3.1 Influence of Surface Roughness on Surface Energy

The surface roughness of the machined samples was measured by means of the confocal laser scanning microscope and the resulting roughness values Sz and Sa are listed in table 2. The roughness values of the X5CrNi18-10 samples have been determined earlier [11]. It can be observed that the roughness of the surfaces of both materials increases from the finely ground surface to the milled surface. Compared with the roughness of the steel samples ranging between Sz = 33.6 µm - 43.6 µm, the roughness of the Ni-based samples is notably lower with values in the range of Sz = 5.1 - 7.1 µm. Also a high deviation from the mean Sz value can be observed for the IN 625 samples. While this deviation is already high for the ground samples, it is still significant after milling. The similar trend can also be observed for the Sa values. While the Sa values of the steel samples were on one level around Sa = 2.5 ± 0.3 µm [11], the roughness of the IN 625 samples ranges between Sa = 0.033 µm - 0.264 µm.

Table 2. Roughness values Sz and Sa of the milled and ground IN 625 and X15CrNi18-10 samples.

		ground 1,200	ground 180	milled
IN 625	Sz	7.5 ± 1.3 µm	6.6 ± 1.6 µm	5.1 ± 1.9 µm
	Sa	0.033 ± 0.003 µm	0.064 ± 0.005 µm	0.264 ± 0.024 µm
X5CrNi18-10 [11]	Sz	33.6 ± 2.1 µm	38.6 ± 4.0 µm	43.6 ± 11.6 µm
	Sa	2.6 ± 0.3 µm	2.3 ± 0.2 µm	2.6 ± 0.5 µm

Figure 1 shows the surface energy of milled and ground X15CrNi18-10 and IN 625 samples calculated from contact angle measurements. As shown before [11], the surface energy of all steel samples amounts to around σ = 40.8 ± 1.4 mN/m with nearly constant disperse and polar shares of $\sigma_{disperse}$ = 26.1 ± 1.8 mN/m and σ_{polar} = 14.4 ± 2.4 mN/m in the analyzed range of surface roughness. In contrast, the surface energy of the Inconel samples shows a notable dependence on the surface roughness. With increasing roughness, the surface energy decreases from around σ = 45.9 ± 0.7 mN/m for the finely ground sample to σ = 35.9 ± 0.7 mN/m for the milled sample. While the amount of the disperse share increases by around 34 %, comparing the finely ground sample to the milled sample, the amount of polar share decreases more significantly by around 90 % to σ_{polar} = 1.77 ± 0.7 mN/m for the milled surface. A possible explanation for this behavior could be that the apparent contact angle θ_a of a liquid changes when applied on a finely structured or very rough surface as explained by Wenzel in [12]. He proposes that a roughness factor r has to be taken into consideration when determining the actual contact angle of the liquid on a finely structured surface. The use of the actual contact angle θ comprising the roughness correction instead of the apparent contact angle θ_a can lead to significant changes in the calculation of the surface energy. The roughness factor is the ratio of the actual surface and the geometric surface and is used as a proportionality factor in the relation $\cos \theta_a = r \cdot \cos \theta$ [12]. Additionally, in some cases for example the hydrophilic characteristics of the system increase with increasing r [13]. This would result in an increase of the disperse shares of the surface energy as it is observed here.

Additionally, further possible explanations have to be taken into consideration. Possibly the predominant direction of the grooves resulting from milling and grinding results in an heterogeneous formation of the surface profile leading to a distorted contact angle of the drop. Furthermore, the different level of thermal stress during milling compared to that occurring in grinding might influence the oxide layer formation on the surface, which would in turn influence the measured contact angle and thus, the apparent surface energy. Currently, the surfaces of the samples are analyzed to identify the relevant mechanism.

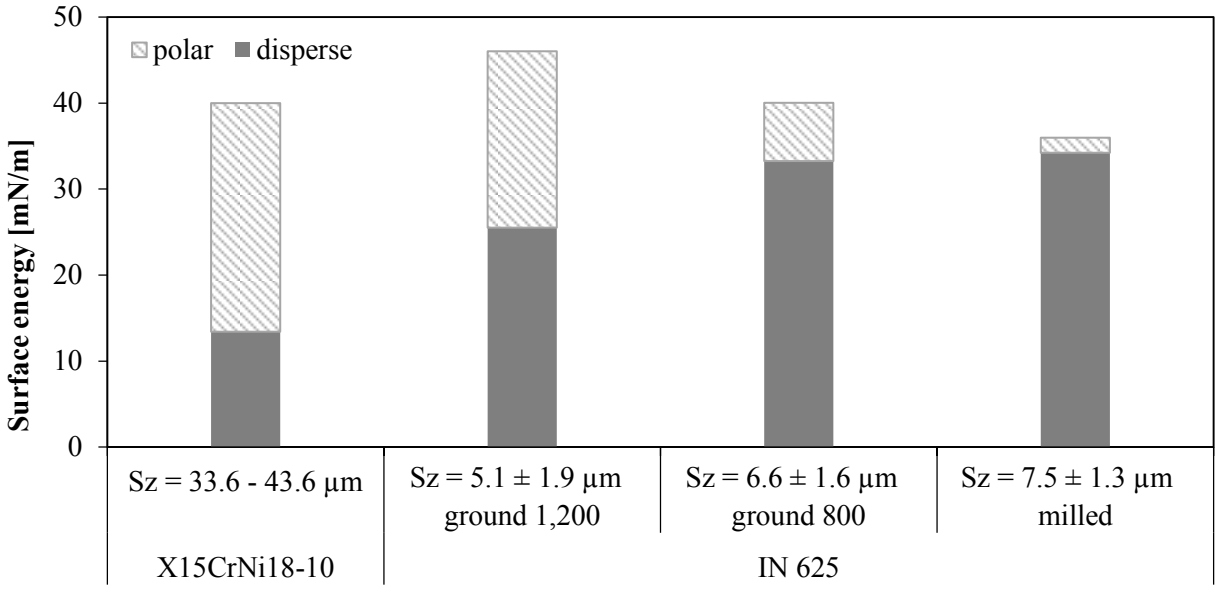

Figure 1. Surface Energy depending on the surface roughness of milled and ground X15CrNi18-10 [11] and IN 625 samples.

3.2 Effect of Plasma Treatment on Cleanliness and Surface Energy

Preliminary tests have shown that plasma treatment alone was not suitable to remove high amount of cooling lubricant residues from the sample surfaces. Using the parameters listed in chapter 2, resulting in short treatment times as known from industrial practice, no effect on the lubricant residues could be optically detected. Even with a high treatment duration of t = 30 s on a fixed position, dark brown, inhomogeneous residues on the surface can be observed. Although higher amounts of carbonic contaminations can be removed from surfaces by repeated plasma treatments, the process is most efficient on pre-cleaned surfaces [14].

Based on the results of the preliminary tests and also based on industrial practice, an alternative cleaning route was chosen. First, the contaminated samples were cleaned by means of the chemical cleaning agents Aceton and IBS respectively, using the cleaning process stated in chapter 2. Afterwards, the plasma treatment was performed. The cleanliness of the samples was determined by fluorescence analysis prior and subsequent to the plasma treatment. Additionally, the samples have been analyzed by Micro-Raman spectroscopy. Figure 2 shows exemplarily the results of the analyses conducted on X15CrNi18-10 samples.

Subsequent to the pre-cleaning with IBS, the measured cleanliness of the samples exhibits already high values of around 96 % (figure 2 a). By the additional plasma treatment, the cleanliness values increase up to 105 % indicating a higher cleanliness level compared to the untreated, clean steel substrate surface used as standard. Additionally, a decrease of the standard deviation of the cleanliness values can be observed leading to the assumption that the plasma treatment results in a surface that is more homogeneous concerning surface composition in comparison to the non-treated surface. Moreover, the Raman spectrograph in figure 2 b) shows the effect of the plasma treatment. The level

of Raman intensity after pre-cleaning with IBS is already very low and no distinct peaks can be observed in the curve. After plasma treatment, the intensity level decreases further indicating a very clean metallic surface as most metals don't show characteristic Raman spectra. For a future brazing process, a clean surface is supposed to be favorable to enhance wetting and flowing of the molten filler metal.

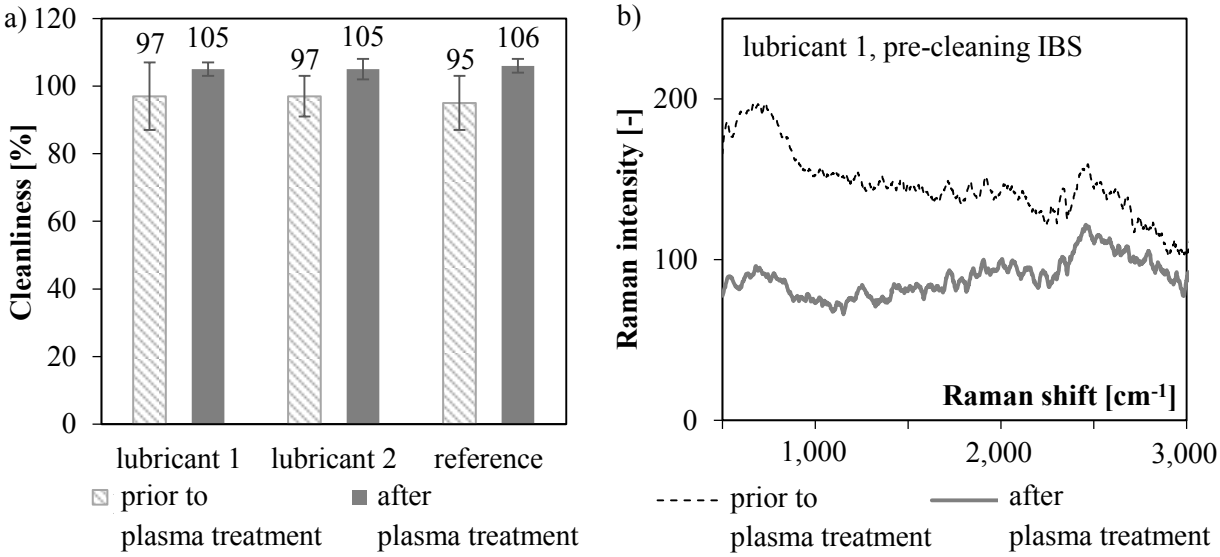

Figure 2. a) Results of fluorescence measurement on pre-cleaned and plasma treated X15CrNi18-10 samples; b) Raman spectrograph pre-cleaned and plasma treated X15CrNi18-10 samples.

In order to investigate the influence of cleanliness on the surface energy of the substrate surface, contact angle measurements were conducted on the pre-cleaned and plasma-treated samples subsequent to a contamination with lubricants. Figure 3 shows exemplarily the results of the IN 625 samples. The results of the plasma-treated samples were first compared with the milled, clean samples from figure 1 as their surfaces were also milled. It can be observed that the surface energy of all plasma-treated samples ranges between 45.7 mN/m $\leq \sigma \leq$ 59.1 mN/m, which is notably higher than that of the originally clean, milled samples with a value of σ = 35.9 mN/m. Furthermore, the amounts of disperse and polar shares differ significantly, as the plasma-treated samples exhibit a notably higher amount of polar shares. However, it can be observed that the level of surface energy and the distribution of the disperse and polar shares of the plasma-treated samples is similar to the clean, finely ground sample from figure 1 with a surface energy of around σ = 45.9 mN/m. This behaviour could probably be partly attributed to the influence of the roughness. As it can be expected that the residues of lubricants accumulate in the grooves and notches of the rough, milled substrate surface, it is very likely that the cavities are filled with residues even after pre-cleaning and plasma-treatment leading to a smoother surface. Thus, the roughness of the surface of the plasma-treated samples on which the contact angle measurements are performed resembles probably more the smooth surface of the finely ground samples. As the roughness is lower, the roughness factor r does not have to be considered for the evaluation of the contact angle measurements, as the apparent and the actual contact angle are similar. Consequently, the surface energy auf the plasma-treated samples is similar to the results of the finely ground sample.

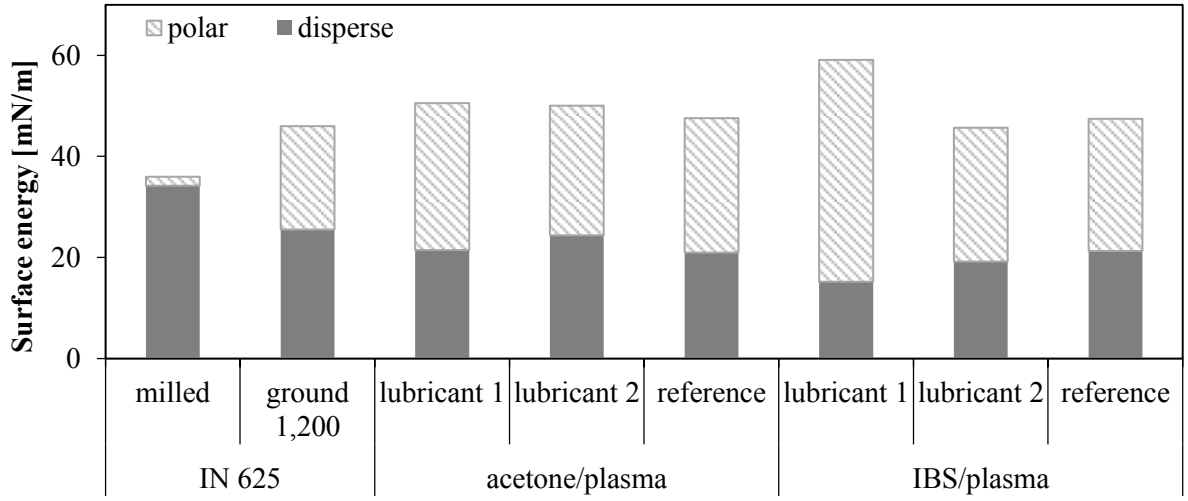

Figure 3. Surface energy of IN 625 samples in machined state as well as in cleaned state following different contaminations.

The disperse shares of the clean, finely ground sample and those of the plasma-treated surfaces are on a similar level of around $\sigma_{disperse}$ = 22.1 ± 2.1 mN /m. However, a higher level of the polar shares of the pre-cleaned and plasma-treated surfaces is reached with values around σ_{polar} = 26.8 ± 1.2 mN/m compared to the finely ground surface with a disperse share of around σ_{polar} = 20.5 mN/m. This is possibly due to the polar residues of the contaminations on the surface based. The sample with the combination of lubricant 1 and IBS pre-cleaning shows the same trend, but more pronounced, with a very low level of disperse share of around $\sigma_{disperse}$ = 15.2 mN/m and a high value for the polar share of the surface energy of around σ_{polar} = 43.9 mN/m.

Previous results on X15CrNi18-10 [11] showed a lower surface energy and a notable reduction of the polar shares after the cleaning process leading to the assumption that the plasma treatment influences the surface energy significantly as well as the amount of polar shares. This is analyzed further on clean samples that are additionally plasma-treated. Furthermore, the influence of the higher surface energy on the wetting and spreading behaviour of the molten filler metal is determined.

3.3 Characterization of the Influence of a Heat Treatment on the Lubricants

The video device for contact angle measurements was used to determine the surface tension of the lubricant. The surface tension of the lubricant 1 containing mineral oil amounts to γ_{lub1} = 31.0 ± 0.4 mN/m at room temperature. The surface tension of the second, synthetic lubricants corresponds to γ_{lub2} = 67.1 ± 0.3 mN/m. As the reference contamination is rather a paste than a liquid, no surface tension could be measured for it. Due to the relatively low surface tension of the first lubricant, it wets the surface homogeneously, even when mixed with the demineralized water. The surface tension of the second lubricant increases further by the addition of water as water has a surface tension of around γ = 72.8 mN/m at T = 20 °C [15]. As a result of the use of the mixture, only partial wetting of the surface is achieved on the sample surface.

Additionally, the lubricants and the reference were analyzed in combined DSC/TG analyses up to T = 800 °C. A high weight loss of 80 % for lubricant 1 and of 60 % for lubricant 2 can be observed in the temperature range between 85 °C ≤ T ≤ 115 °C (figure 4 a). This weight loss coincide with an endothermic peak in the heat flow curve in figure 4 b in the temperature range between 20 °C ≤ T ≤ 150 °C. The peak of lubricant 1 is divided in two peaks indicating two different reactions. The first reaction at around T = 100 °C is probably correlated with the evaporation of water and the second one with the evaporation of volatile components of the lubricants. The fact that the second lubricant doesn't exhibits the strong second peak leads to the lower weight loss. Between 115 °C ≤ T ≤ 400 °C the second lubricant shows another but less pronounced step of weight loss

resulting in a total weight loss of 77 %. The reference contamination doesn't show neither weight loss nor heat flow peaks at lower temperatures. In the temperature range between 200 °C ≤ T ≤ 500 °C, several small endothermic peaks can be seen in the heat flow curve resulting in a pronounced decrease of weight of around 78 %. It can be concluded that after a heat treatment up to T = 800 ° C, around 10 % - 20 % of the original weight of the lubricants can be found on the surface. These residues can be observed on the sample surfaces in the form of dark, crumbly and voluminous material. Based on the structure and appearance of the residues, it can be assumed that some graphitic material has been formed.

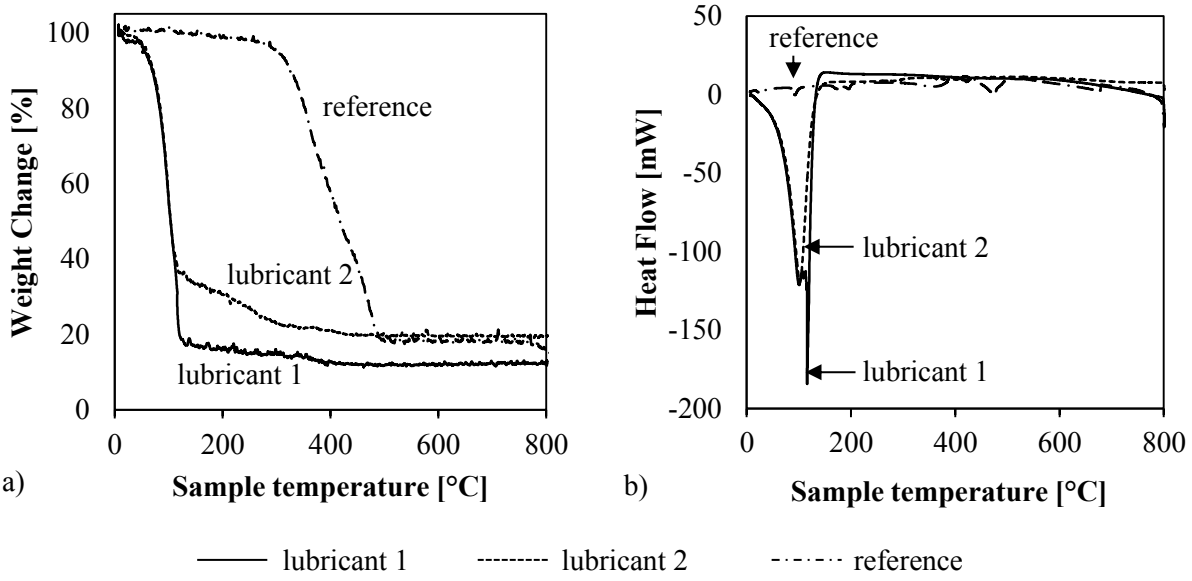

Figure 4. a) Weight change and b) heat flow during combined DSC/TG analyses of lubricants 1, 2 and reference in the temperature range 20 °C ≤ T ≤ 800 °C.

In order to identify the dark, crumbly residues resulting from the heat treatment of the lubricants, Micro-Raman measurements were done on fresh lubricants as well as on heat-treated samples showing the residues on the surface. Figure 5 shows exemplarily the results of the analyses of X15CrNi18-10 samples. Comparable results were observed for IN 625. This was expected because no intense chemical interaction should occur between lubricant and base material. In figure 5 a) hardly any peaks can be detected for the fresh lubricants possibly due to an amount of moisture in the material.

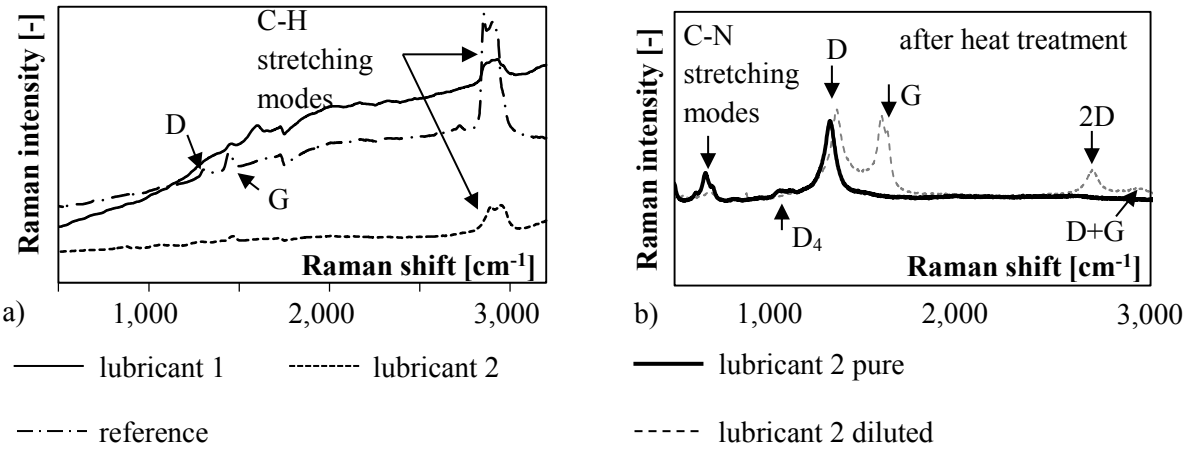

Figure 5. Raman spectrographs of a) fresh lubricant 1, 2 and reference b) heat-treated pure and diluted lubricant 2, both on X15CrNi18-10.

In the range of the Raman shift between 2,800 $cm^{-1} \leq \tilde{\upsilon} \leq 3{,}020\ cm^{-1}$, broad and flat peaks can be found for lubricant 1 and 2 and peaks with higher intensity for the reference. Peaks in this range are due to C-H stretching modes indicating the existence of partly long-chain hydrocarbons containing CH_2 or CH_3 groups [16]. Peaks at Raman shifts of $\tilde{\upsilon} > 3{,}000\ cm^{-1}$, can be assigned to complex nitrogen containing hydrocarbon groups [17]. Additionally, some small peaks can be seen at around $\tilde{\upsilon} = 1{,}367\ cm^{-1}$ and at around $\tilde{\upsilon} = 1{,}540\ cm^{-1}$ indicating sp^3 and sp^2 carbon bonds [18, 19]. Their intensity is comparatively low due to the high intensity of the peaks for the C-H stretching modes. The band correlated to sp^3 is shifted to a higher frequency compared to the diamond sp^3 band at $\tilde{\upsilon} = 1{,}332\ cm^{-1}$. Especially in graphene based material, peaks in the range of $1{,}330\ cm^{-1} \leq \tilde{\upsilon} \leq 1{,}360\ cm^{-1}$ are called the D band. This peak occurs when the graphene sheets are irregularly stacked in graphite, when defects at the edges or in the plane of the two dimensional graphene stacks exist. The second peak is correlated with the primary phonon G band, typically located at around $\tilde{\upsilon} = 1{,}580\ cm^{-1}$, indicating the carbon lattice stretching in the plane of the graphene sheets. A shift of this peak can be correlated with different interactions between the graphene layers and a change of the peak form can be attributed to a splitting of the peak due to several underlaying band with slightly different energies and frequencies [18].

Figure 5 b) shows the Raman spectrograph of pure and diluted lubricant 2 after heat treatment. It can be noted that the peaks of the spectrographs are relatively broad. This can be attributed to a highly defective structure of the graphene sheets, but also to the amount of sheets that are stacked. It could also be possible that the broading of the peaks is a result of amorphous carbon in the material. But as the cooling rate of the samples is low, the formation of a higher amount of amorphous material is not expected. The position of the peaks and also the relation of the intensities observed here is very similar to another study where the degree of crystallinity and number of the graphene layer increased with decreasing cooling rate leading to broad peaks [20].

While the spectrograph of the different contaminations is characterized only by some C-H stretching modes indicating the existence of long-chained hydrocarbons, more defined peaks can be seen after heat treatment. Especially in the spectrograph of the diluted lubricant, the D band at around $\tilde{\upsilon} = 1{,}360\ cm^{-1}$ and the G band with a doublet at around $\tilde{\upsilon}_1 = 1{,}600\ cm^{-1}$ and around $\tilde{\upsilon}_2 = 1{,}620\ cm^{-1}$ can be seen. Additionally, the 2D(G') band can be observed at around $\tilde{\upsilon} = 2{,}720\ cm^{-1}$ due to secondary phonons resulting from the same defects as the D band. Furthermore, at higher Ramans shift of around $\tilde{\upsilon} = 2{,}900\ cm^{-1}$ a new band occurs known as the D + G band. It results from a double resonance scattering process and is also induced by the defects in the graphen structure. The

spectrograph of the pure, heat-treated lubricants shows fewer and slightly different peaks. It shows only pronounced peak at around $\tilde{\upsilon} \leq 1{,}340$ cm^{-1}, comparable to the D band of the pure lubricant but slightly shifted to lower frequencies. Furthermore, at around $\tilde{\upsilon} = 1{,}200$ cm^{-1}, a broad but flat peak can be observed which is attributed to the D_4 band. This band occurs in highly defective carbons and have been related to hydrocarbons or residues of aliphatic compounds connected with the graphitic structure. A small peak at around $\tilde{\upsilon} = 700$ cm^{-1} can be attributed to C-N stretching modes [17].

Summarized it can be concluded that the long-chained hydrocarbons in the lubricants react during the heat treatment to graphene-based compounds, for example graphite, especially when the lubricant has been diluted with demineralized water. Due to the higher intensity of the D band, it can be concluded that the structure is highly defective possibly due to distortions during stacking or defects at the edges of the graphene sheets. A difference between the pure and diluted lubricant can be seen as the spectrograph of the pure lubricant shows more indication of residues of aliphatic hydrocarbons and of C-N bonds. These different kinds of residues on the sample surfaces can lead to different wetting behavior by the molten filler metal in a brazing process. It has been shown before that residues of the lubricants and cleaning agents on the surface lead to an enhanced spreading of the filler metal [11].

4. Conclusion and Outlook

The analyses of the sample surfaces by means of confocal laser scanning microscope showed an influence of the roughness of the IN 625 samples on their surface energy. The surface energy and especially the disperse share of the energy increased with increasing roughness. This could be attributed to the necessity to take into account the roughness factor developed by Wenzel for finely structured surfaces. Differences in the flowing behaviour of filler metals on these surfaces can be expected due to the enhanced spreading of the filler metal on substrates with residues of lubricants and cleaning agents shown before [11]. The flowing behaviour of the filler metal on heat-treated samples is currently analysed in detail.

Additionally, it could be seen that a pre-cleaning process combined with a plasma treatment of the samples could further increase the cleanliness of the surfaces. Thus, a reduction of voids and defects and inclusions of lubricant residues in the brazed joint can be expected enhancing the quality of the joints. Furthermore, the surface energy and especially its polar share are increased after the pre-cleaning and plasma treatment. The influence of this increase on the wettability and spreading of a molten filler metal is also currently determined.

The analyses of the behaviour of the lubricants show a strong reaction during a heat treatment similar to that occurring during the actual brazing processes. While a high amount of the former fresh lubricants, consisting mostly of long-chained hydrocarbons, evaporate during the heat treatment, around 20 wt.-% remain on the surface but mostly as a graphene-based compound, probably in the form of graphite. Raman spectrographs indicate that the graphite structure is disordered and defective leading to a voluminous and crumbly structure on the surface. The graphitic structure is a challenge for a brazing process as it is difficult to wet. Additionally, the crumbly structure will be included in the braze material leading to a reduction the mechanical properties. Also the difference between the residues of pure and diluted lubricants has to be further analyzed regarding the wettability of both kinds of residues by a molten filler metal.

Acknowledgement

The project IGF 18387 N of the research association German Welding Society (DVS) is funded by the AiF within the framework of the program to promotion of the IGF (Industrielle Gemeinschaftsforschung) by the German Federal Ministry for Economic Affairs and Energy according to a resolution of the German Bundestag. The authors would also like to thank the project partners from Institute of Materials Engineering for the good cooperation.

References

[1] Hertlein K 2000 *Reinigen mit Kohlenwasserstoff-Lösemitteln und Wasser im metallbearbeitenden Gewerbe, im Druck- und Elektronikbereich* ed W J Bartz and E Wippler *(*Renningen-Malmsheim: Expert-Verlag)
[2] Grün R 2005 *reprinting STAHL Heft* **2** 35–38
[3] DIN 5892:2003 *Manufacturing processes cleaning – classification, subdivision, terms and definitions*
[4] Kegel B and Schmid H 1999 *Surf. Coat. Technol.* 112(1) 63–66
[5] Adams H-N and Jelinek T W 1999 *Reinigen und Entfetten in der Metallindustrie,* ed T W Jelinek (Bad Saulgau: Eugen G. Leuze Verlag)
[6] DIN EN ISO 28178:2016 *Geometrical product specifications (GPS) - Surface texture: Areal*
[7] Oberhausen M 2007, Dissertation Universität Saarbrücken
[8] Schütz A and Triebert J 2008 *Metalloberfläche* **62** 29–31
[9] Lugscheider E and Bobzin K 2003 *Surf. Coat. Technol.* **165** 51–57
[10] Mantel M and Wightman J P 1994 *Surf. Interface Anal.* **21** 595–605
[11] Bobzin K, Öte M, Wiesner S, Tillmann W, Wojarski L, Manka M and Eilers A 2016 *Proc. of 11thInt. Conf. on Brazing, High Temperature Brazing and Diffusion Bonding LÖT 2016,* 7th - 9th June 2016 (Aachen) in *DVS Berichte* **325** (Düsseldorf: DVS Media GmbH), 128–132
[12] Wenzel R N 1936 *Ind. Eng. Chem.* **28** 988–994
[13] Quéré D 2005 *Rep. Prog. Phys.* **68** 2495-2532
[14] Saito H, Shiki H, Tsjii K, Oke S, Suda Y, Takikawa H and Amanaka S 2009 *Jpn. J. Appl. Phys., Part 1* **48.8S1** (2009) 08HH03
[15] Harkins W D and Brown F E 1919 *J. Am. Chem. Soc.* **4** 499–524
[16] Spiker R C, Levin J R and Levin I W 1975 *Biochim. Biophys. Acta* **338** 361–373
[17] Garber B P and Peticolas W L 1977 *Biochim. Biophys. Acta* **465** 260–274
[18] Hodkiewicz J 2010 *Thermo Scientific Application Note* 51946 (2010)
[19] Bokobza L, Brunel J-L and Couzi M 2015 *C* **1** 77–94
[20] Li C, Li D, Yang J, Zeng X and Yuan W 2011 *J. Nanomat.* 19624